

We are IntechOpen, the world's leading publisher of Open Access books Built by scientists, for scientists

6,900

Open access books available

186,000

International authors and editors

200M

Downloads

Our authors are among the

154

Countries delivered to

TOP 1%

most cited scientists

12.2%

Contributors from top 500 universities



WEB OF SCIENCE™

Selection of our books indexed in the Book Citation Index
in Web of Science™ Core Collection (BKCI)

Interested in publishing with us?
Contact book.department@intechopen.com

Numbers displayed above are based on latest data collected.
For more information visit www.intechopen.com



Behavior and Design of Transfer Slabs Subjected to Shear Wall Loads

*Alonso Gómez-Bernal, Eduardo Arellano Méndez,
Luis Ángel Quiroz-Guzmán, Hugón Juárez-García
and Oscar González Cuevas*

Abstract

This paper investigates the behavior of a transfer slab system used in medium rise building. For this purpose, two slab-wall full-scale specimens were designed, built, and tested to cyclic loads. The two slab-wall prototypes were exposed to three load stages: (a) vertical load, (b) horizontal load, and (c) vertical and horizontal combined load. The first specimen, SP1, includes a masonry wall situated on top of a squared two-way slab of 4.25 m by side, thickness of 12 cm, on four reinforced concrete girders, while the second specimen, SP2, consists of an identical slab but was constructed with a reinforced concrete wall. Some numerical finite element slab-wall models were built using linear and nonlinear models. The most important results presented herein are the change on lateral stiffness and resistance capacity of the load-bearing wall supported on a slab versus the wall supported on a fixed base and the effects that these walls cause on the slabs. During the experimental test process of horizontal loading, we detected that the stiffness of the two slab-wall systems decreased significantly compared to the one on the fixed base wall, a result supported by the numerical models. The models indicated suitable correlation and were used to conduct a detailed parametric study on various design configurations.

Keywords: transfer slabs, transfer floor system, discontinuity in buildings, shear walls on slabs, slab experimental behavior

1. Introduction

1.1 Buildings with transfer slab systems

In Mexican cities the construction of medium-rise buildings with a structural floor system called “transfer slabs” have been popularized in the last 15 years. A study [1] evaluated a set of buildings constructed in a sector of Mexico City, in this evaluation was detected a high percentage of buildings that were constructed with discontinuous walls, a structural configuration that induced irregularities in several buildings. These structures, projected with transfer floor systems represent a high risk, because it is known that buildings with discontinuity in elevation are vulnerable to seismic loads. This situation is critical when load-bearing walls,

especially on the first floor, are not aligned with the vertical forces, therefore increasing seismic vulnerability.

The buildings designed with transfer slab (or transfer floor) have a floor system supported on one rigid level, which is used as a parking lot. On top of this transfer slab is constructed a shear masonry walls super-structure of more than four stories. A significant percentage of these walls are interrupted at transfer floor level and are discontinuous in the foundation. Nevertheless, a few walls in the boundaries of the structure are continuous until the base, but many walls in upper stories are not aligned with the framed axes of the bottom story. Numerical models have demonstrated that this structural configuration produces a significant increase in the shear stress in discontinuous walls, as is discussed in detail in Ref. [2]. This can be explained due to the excessive deflections that walls provoke to slab. Shear forces calculated are between two to three times larger than those that these walls would have if they were continuous along all their height. Besides, the transfer slab is exposed to additional high deformations and stresses.

During the September 19, 2017 earthquake ($M = 7.1$) an extensive damage was observed in Mexico City, some buildings structured with transfer slab system suffered important damage [3]. For example, **Figure 1a** show the total collapse of a building located in the Lake bed zone which had eight stories, the structure was located at the corner of a block, only the ground story consisted of reinforced concrete frames, while the upper stories were structured only with masonry walls conforming a structure with high discontinuity in elevation; this building collapsed due a high irregularity killing 5 residents. **Figure 1b** shows other two cases that correspond to two modern buildings structured with this transfer floor system, when these structures were reviewed, minor diagonal cracks were detected at the ends of the girders of the floor transfer (**Figure 1b**), in one of these buildings residents were evicted.

The structural system based on transfer floors requires a major research. In the literature exists a great number of experimental studies on the performance of load-bearing walls subjected to horizontal forces that has been characterized the seismic effects. Walls that have different parameters, in terms of materials, steel reinforcement, load conditions and other properties have been tested [4–7], and some of the most notable results were documented [8]. Nevertheless, in terms of performance of RC slabs, there is less information due to the limited number of experimental programs [9–11]. In these studies, the walls are fixed in their base and slabs were subjected to distributed or concentrated loads; however, there was no specific information about linear loads applied directly on the slabs, i.e. slabs supporting walls. The behavior between a building structured with transfer floors and one traditional



Figure 1. (a) left: Collapse of a building with discontinuities in elevation; (b) right: Diagonal cracks in the girders of the transfer floor in two buildings supporting six and seven stories, respectively.

(without discontinuous walls) is different. For this reason, was implemented our experimental program.

1.2 Objective and scope

The objective of this study is to develop an experimental and a numerical program that considers the interaction between a wall and the slab on which is supported. In the experimental program, two full-scale slab-wall specimens were designed, assembled, and tested by cyclic loads in the Laboratory of Structures at UAM. The prototypes slab-wall were exposed to three load stages: vertical load, horizontal load, and combined vertical and horizontal load. The first specimen, SP1, include a masonry wall situated on top of a squared two-way slabs, while the second specimen, SP2, consists of an identical slab but was constructed with a reinforced concrete wall. To support the experimental results, and characterize the behavior of transfer floor structures, some numerical finite element slab-wall systems were analyzed using linear and nonlinear criteria.

2. Experimental program

2.1 Tested specimens, SP1 and SP2

Two slab-wall specimens were constructed in the experimental program. This program included three load stages: (a) vertical loads representing the vertical load component detected in buildings structured with floor system, (b) horizontal cyclic loads applied at low load levels in order to investigate the linear response, and (c) combined constant vertical and horizontal loading cycles.

Specimens SP1 and SP2 consist of four reinforced concrete perimetral girders with a solid two-way slab which together conform a monolithic structure. These girders have a transversal section of 25×70 cm, and the slab is square of 425×425 cm and 12 cm thick, the slab plane is located at 77 cm over the laboratory floor (see **Figure 2**). The concrete strength was $f'_c = 250$ kg/cm². The two beams aligned transversals to the wall are haunched girders, while the two girder parallels to it have a rectangular section. The haunched girders were used to adjust the specimen to the conditions of the laboratory's reaction floor, and the position of the laboratory's horizontal load reaction system. The design and steel reinforcement in the slab were determined using typical procedures, such as the ones used in real buildings in Mexico. On the outer strips, the spacing of the bottom re-bars was set to 40 cm. On the central strip, the spacing was set to 20 cm in both directions. In the top of the slab, the reinforcement spacing was also set to 20 cm. **Figure 3** shows details of the reinforcement used in the slab specimens.

The first specimen, SP1, include a masonry wall placed on top of the slab. This wall is 2.50 m wide by 2.41 m high, was constructed on the slab's central strip. The wall is confined with two tie-columns, 14×18 cm, and with a tie-beam, 14×14 cm. The bottom tie-beam was integrated with the slab. The concrete resistance of the tie-columns was $f'_c = 150$ kg/cm², with four re-bars in the corners. The re-bars are conformed with the minimum steel requirements of the Mexico Construction Code for masonry structures [12].

The second specimen, SP2 (**Figure 2**), consists of a slab with a Reinforced Concrete (RC) wall, reinforced with electrowelded wire mesh, besides at the ends were placed tie columns. The wall was placed on top of a squared two-way slab, with the same characteristics of SP1 specimen. The RC wall is 2.50 m wide by 2.40 m high, and with a thickness of 10 cm (top-right of **Figure 3**).

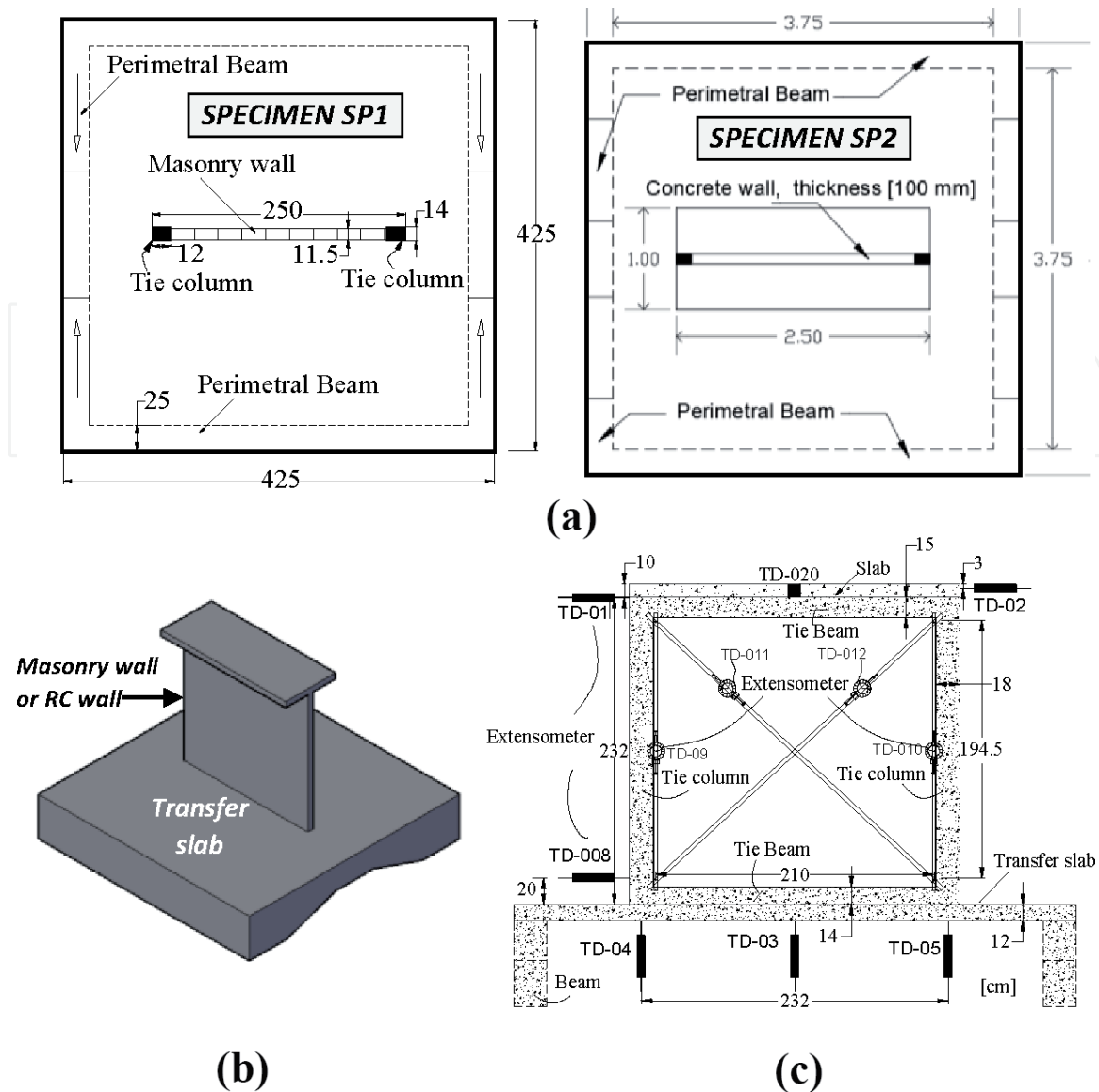


Figure 2. Geometry and details of slab-wall specimens SP1 and SP2: (a) plan view of specimens; (b) transfer slab 3D model; (c) location of exterior instrumentation.

2.2 Setup, devices, instrumentation, and loading scheme

Three mechanical steel devices were designed and built to develop the experimental program: the first for attachment purposes, the second one for simulate the gravitational loading, and the third one for the lateral cyclic loading. The attachment device prevented the slab-wall specimen from moving in a vertical or lateral way during the test whenever the loads were applied to the wall. The vertical load device was fabricated by a system of steel girders, eight tensors and their anchorages (see **Figure 4**). At the top of the girders there are four vertical actuators (each with a 25 Ton capacity), supported on a base plate, which keeps them in an upright position and prevents them from slippage. The third device was designed for the incremental cyclic horizontal loading. We used a double-action hydraulic actuator with a 25 Ton push capacity, and a 13 Ton pull capacity. A more detailed description can be found in [13].

The interior instrumentation consists of a set of strain gages (SGs) that were installed in the reinforcement bars of the concrete elements. In specimen SP1, 16 SGs were fixed in the bars of the bottom of slab and 16 SGs in the top (**Figure 3**). The tie-columns of the masonry wall had 20 SGs in the longitudinal re-bars. Additionally, 10 SGs were embedded in the concrete slab and the tie-columns. In specimen SP2,

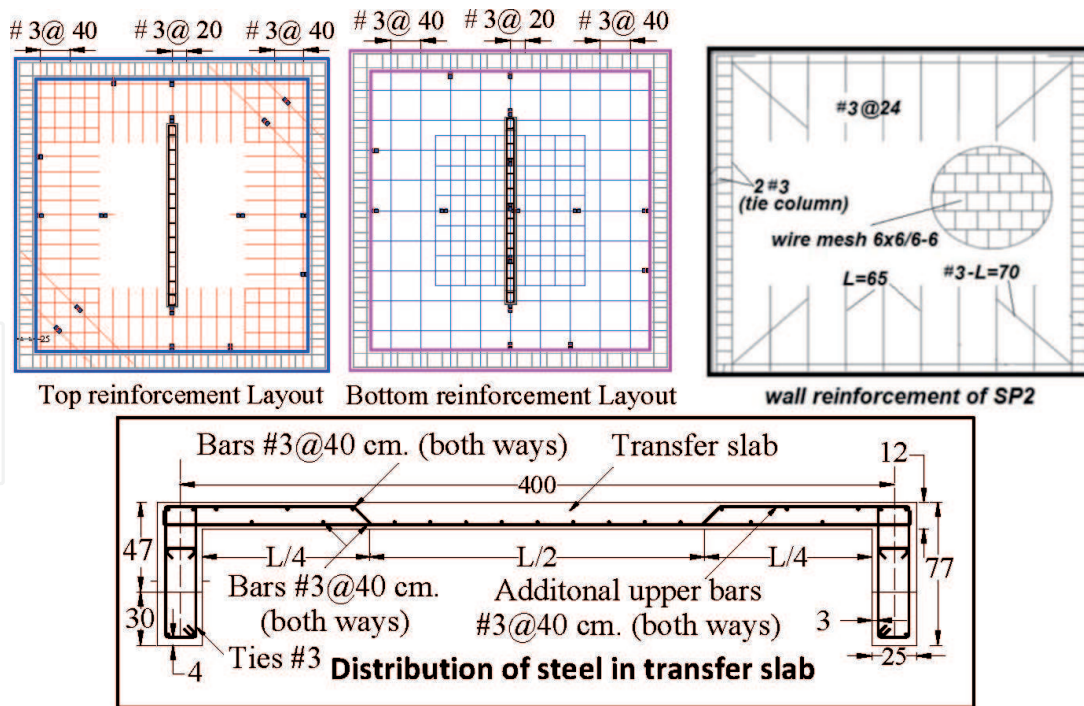


Figure 3. (Top) Reinforcement details in transfer slab and reinforced concrete wall of SP2; (Bottom) assembly of strain-gages in bars is included.

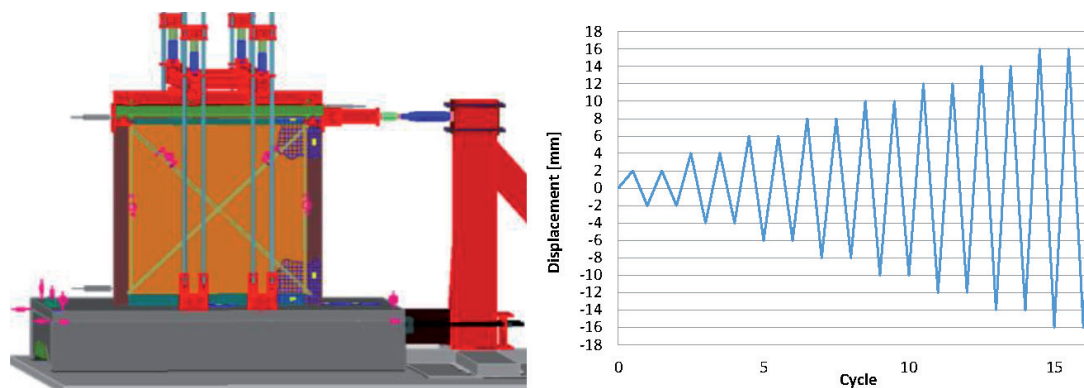


Figure 4. Test set-up and typical displacement time history (horizontal loading).

a total of 48 SGs were fixed along the longitudinal and transversal directions of the reinforced bars.

The exterior instrumentation consisted of two parts, first, in order to measure the forces applied through the hydraulic cylinders, load cells (LVDT's) were attached (four verticals and one horizontal); and second, 20 transducers (TDs) were installed at strategic points with the purpose to measure the vertical and lateral deflections.

Figure 2c shows the TDs on the lower face of the slab. The TD that provides the most relevant information is TD03 because it is in the center of the slab, exactly below the center of the wall (masonry in SP1, or concrete in SP2). The TD03 transducer is used as a control node to determine vertical displacements.

3. Numerical models

In a previous work [2], numerical inelastic models for the slab-wall system were studied using finite element (ANSYS [14]). Twelve detailed geometries were

analyzed, six models were defined for wall masonry, and six systems for reinforced concrete wall. **Table 1** shows the geometric characteristics of six studied models, four different wall lengths and two slab thicknesses were used. The model was divided in two sections for reducing computational time in analysis. The support conditions of the slab are theoretically restricted along the perimeter. The models M10_M2.5_12V, M10_M2.5_12VL, M1_C2.5_12V and M9_C2.5_12VL are like the tested specimen.

All slab-wall numerical models were subjected to two load conditions, first to an incremental vertical load, and second to a combined load consisting of a simultaneous constant vertical component with incremental cyclic horizontal load. Capacity curves for the systems were generated with the obtained results. In addition, for comparison purposes, analysis of the vertical load condition included a slab model (without wall) subjected to a uniform load. For horizontal load analysis, a nonlinear model with wall on a rigid basis was used for comparison purposes (flexible base wall).

4. Definition of specimen response

In order to define force-deformation behavior and the different damage states of the two tested specimens, it is necessary to establish the deformation modes or configurations for each of the three load protocols studied (**Figure 5**). Therefore, the failure in the walls of the specimens, SP1 and SP2, will depend on the bending (ΔF) and shear (ΔC) deformations induced by horizontal loading. However, in this case, since each wall is supported by a slab, the lateral displacement due to the wall rotation (ΔL), induced by the slab deformation, must be considered. Total displacement, ΔT , at the top of the wall is then generated and presented in **Figure 5**.

Shear deformations of the walls can be obtained from recorded deformations of transducers installed in diagonal directions. Based on the strength of materials theory, the unitary angular deformation, γ is due to the shear stress acting on the wall element [4]. In general, this deformation is defined by the following expression:

$$\gamma = \frac{\delta_2 L_2 - \delta_1 L_1}{2l_m h_m} \quad (1)$$

where γ = angular deformation of the wall, δ_1, δ_2 = shortening or elongation measured on the diagonals, L_1, L_2 = initial length of diagonals, l_m, h_m = are the width and height of the wall, respectively.

And the total distortion (R_{tot}) or effective distortion (R_{Eff}) is calculated as:

$$R = \Delta E / H \quad (2)$$

$$\Delta E = \Delta F + \Delta C - \Delta L \quad (3)$$

$$\Delta L = (\Delta I - \Delta D) \times H / L \quad (4)$$

where R = effective drift of the wall, ΔE = effective lateral displacement at top of the wall, ΔL , ΔF , and ΔC are defined in **Figure 5**, ΔI , ΔD are vertical displacements at ends in wall-slab joint, H = distance between TD-01 y TD-08 (**Figure 2**), L = distance between TD-04 y TD-05 (**Figure 2**).

Concrete wall model	Masonry wall model	Wall width (m)	Slab depth (cm)
M1_C2.5_12V	M2_M2.5_12V	2.50	12
M3_C3_12V	M4_M3_12V	3.00	12
M7_C3_13V	M7_M3_13V	3.00	13
M9_C2.5_12VL	M10_M2.5_12VL	2.50	12
M11_C3_12VL	M12_M3_12VL	3.00	12
M15_C3_13VL	M16_M3_13VL	3.00	13

Table 1.
 Code for slab-wall numerical models [2].

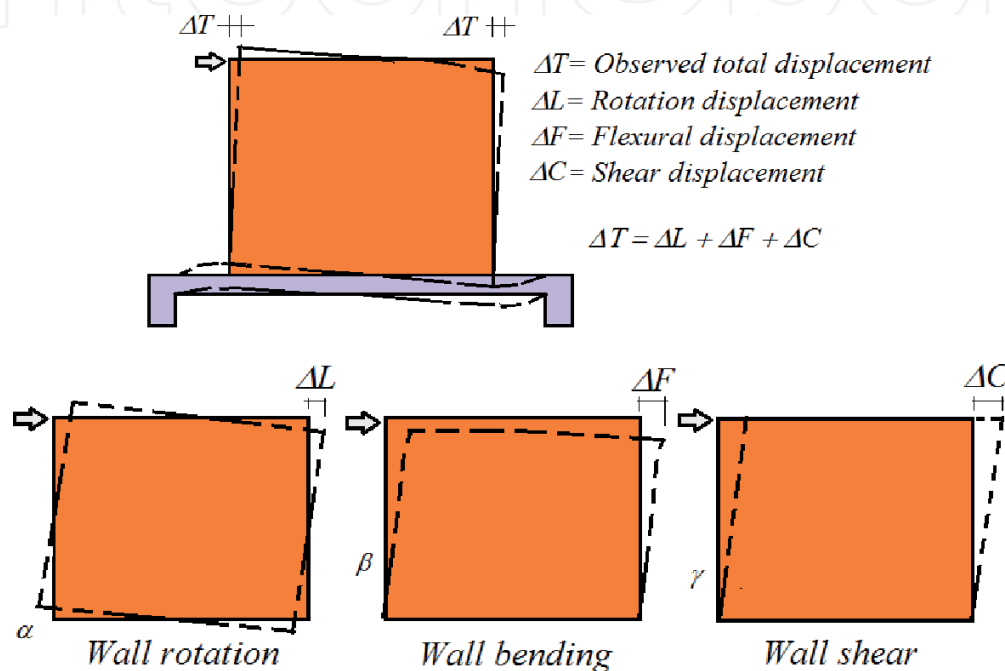


Figure 5.
 Total deformation (above) and principal deformation modes.

5. Experimental and numerical results

5.1 Response to vertical loading, experimental vs. numerical results

In **Table 1** are defined the key to numerical models as: M#_Mat#_#V. The M# indicates the model number. The Mat# indicates the material and length of the wall, for example M3.0 indicates that the wall material is Masonry, and has a length of 3.0 m, while C indicates that the material wall is Reinforced Concrete. The #V indicates the slab thickness, for example 13 V indicates that the slab is 13 cm thick.

The experimental (Exp) capacity curve of SP1 is compared with the numerical model curve (M2_M2.5_12V). It can be observed that in the experimental case a minor stiffness value is obtained, as is observed in the curve. This situation can be explained due to the perfect fixed ends along the slab perimeter in the numerical model. But in both capacity curves, the first slab cracking occurred at the same time. This occurs when the load reached a value of 5.5 Ton (**Figure 6**). Numerical model, M2_M2.5_12V, was conducted until the failure condition, the first slab cracking take place at 5.5 Ton; the whole structure exhibited linear behavior until the ultimate load of 25 Ton. At this point an almost perfect elastoplastic “nonlinear” performance was detected (**Figure 6**).

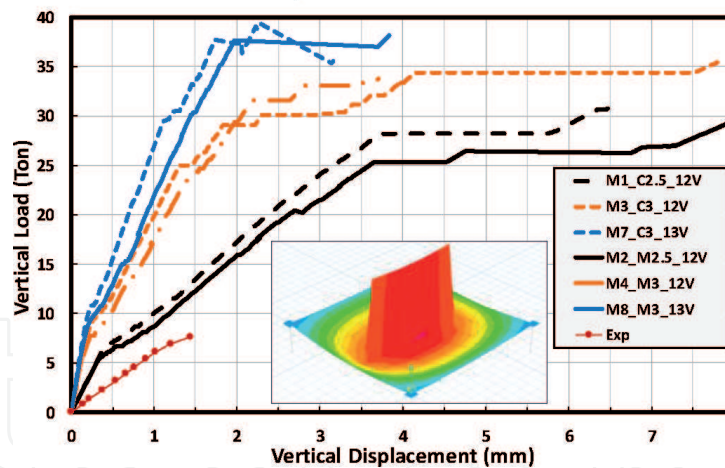


Figure 6.
Capacity curves obtained from numerical and experimental models, subjected to vertical loading.

When the capacity curves of numerical models M1_C2.5_V12 (reinforced concrete) and M2_M2.5_12V (masonry) are compared, they have a similar trend. This behavior indicates that under gravitational loading, no matter what material the wall is made of, the capacity of the whole structural system will almost remain the same. This result is corroborated with the other two pairs of curves shown in **Figure 6** (for example M3_C3_V12 and M4_M3_V12), which also described the same trend. When the wall length or slab thickness (M7_C2.5_V13 and M8_M2.5_V13), were increased the ultimate capacity was also increased. One important result obtained from the numerical study is that when the slab thickness is increased in models, the ultimate model capacity also increases. Before the first crack occurs, it can be assumed to be a service condition, the observed stiffness in the models during this condition were similar, and hence a thicker slab does not ensure a significant stiffness value.

5.2 Response to vertical and lateral loading

Specimens SP1 and SP2 were exposed to a constant vertical load of 8 Ton plus 16 cycles of monotonic horizontal loading. The loads were applied with hydraulic jacks with the skill to apply push and pull actions. The loading was controlled by the lateral displacement at wall top. The 16 cycles (**Figure 4**) were applied in pairs (push and pull actions), from 0.5 to 12 mm; for the specimen SP1, the last two cycles were asymmetric (14 and 27 mm), due to the limitation of the hydraulic jack in performing pull actions. The associated applied loads were above 11 Ton and 9 Ton in push and pull actions. For specimen SP2, the hydraulic cylinder was changed to have the same load capacity in pull and push.

5.2.1 Displacement and rotation of the wall

The vertical transducers TD05, TD03, and TD04, located under the specimen slab, were used to measure the vertical displacements during the test. These transducers were installed along the centerline under the wall (**Figure 2**). Due to the effect of horizontal loading, each time the right transducer (TD05) rises above the original reference line, a rigid body wall rotation occurred (**Figure 3**). We observed a considerable increased in the vertical displacement with every incremental load cycle, indicating that due to the intensity of the vertical load on the slab, the observed overall structural performance was nonlinear. In each cycle, the slab

experienced a displacement of 0.5 mm without returning to its initial position. This represented a cumulative displacement of approximately 9.5 mm at the end of test.

5.2.2 Shear strains

The wall rotation, γ , caused by shear deformations in specimen SP1, is established according to the mechanics of materials theory. Because transducers installed in the wall diagonals did not register any deformation during the first stage of the loading process (first six loading cycles), therefore, it can be concluded that the wall did not develop any shear strains in this phase. As a consequence of slab rotation, the wall only experienced base rotation and bending. But, in the seventh cycle, diagonal transducers, TD011 and TD012, began to register shear strains. Still until the tenth cycle, the masonry wall behaved linearly, but later the wall suffered nonlinear deformations.

5.2.3 Global and relative horizontal drifts

The total distortions, R_{tot} , and the relative drift, R_{eff} , of specimen SP1, measured in the combined loading are illustrated in **Figure 7**. The envelopes of the hysteretic cycles are also shown, which are estimated with the bilinear behavior of the curves. The rigidity of SP1 was defined from the slopes of the curves; the stiffness of the complete system was determined to be equal to 11.3 Ton/cm, while the rigidity of the isolated wall was assessed to be equal to 40 Ton/cm (the effect of the rotation as a rigid body was removed). This stiffness is 3.5 times greater than that due to the wall resting on a flexible base (wall placed on the centerline of a two-way slab).

For second specimen, SP2, it can be observed that the slab rotation is practically equal to the wall bending (**Figure 8**). It can be concluded that the wall did not have any shear deformation.

In **Figure 8**, four limits are proposed to define the behavior of the specimen SP2. A behavior without damage (green color), a behavior with moderate damage (yellow color), a behavior with serious damage that can be repaired (orange color) and a behavior with serious damage that cannot be repaired (red color).

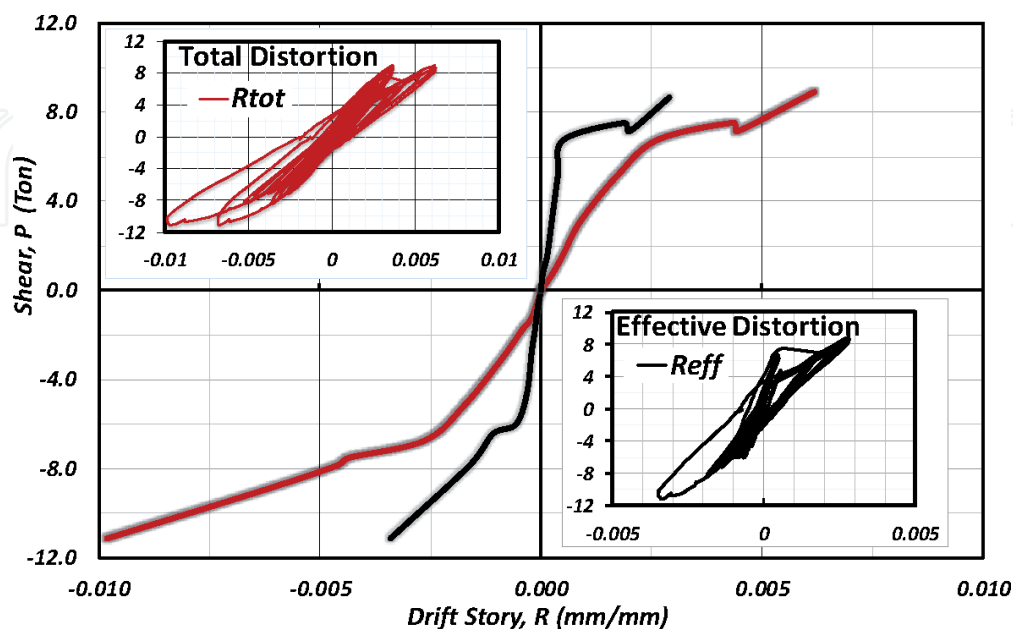


Figure 7. Global (R_{tot}) and effective (R_{eff}) distortions of specimen 1 (with masonry wall) during the combined load, as well as their respective envelopes.

The experimental stiffness for the second specimen (SP2) was calculated from the slopes of the curves; the stiffness of the slab-wall system was estimated as 10.45 Ton/cm, this value is less than the first specimen (SP1) because the slab had damage prior to the beginning of the experiment.

In **Figure 9** are made two comparisons: first, the numerical capacity curve “Effective FEA” (or MBR_M2.5 masonry wall on rigid base) is compared with experimental curve SP1 “Effective EXP”; and second, the numerical capacity curve “Total FEA” (or M10_M2.5_12VL masonry wall on flexible base) with experimental curve SP1 “Total EXP”. The comparison between pairs of curves indicates that these are similar at low levels of load, but when comparison is made between rigid and

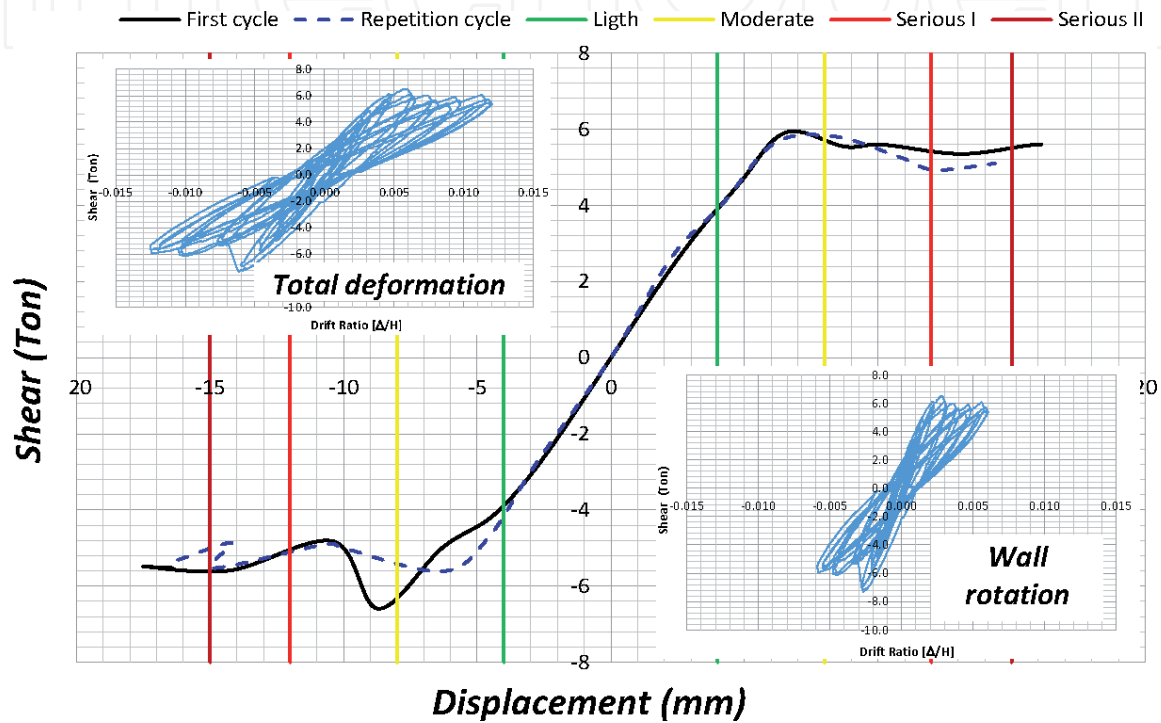


Figure 8. Distortions of specimen SP2 (RC wall) due to the combined load, as well as their respective envelopes.

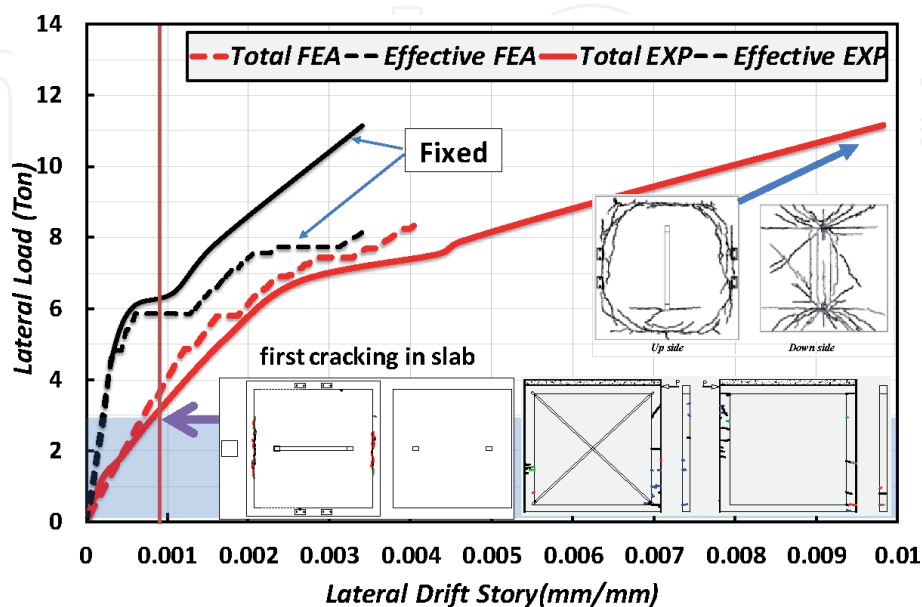


Figure 9. Comparison between numerical and experimental model SP1. Experimental flexible base (total) and rigid base (effective) versus numerical behavior.

flexible base, we observed significant differences between the slopes of the curves. Then, stiffness results indicated that for a wall on a flexible base a value of 14 Ton/cm was reached, while the one on rigid base was computed as 40 Ton/cm, this represent a ratio of 3 times between both cases. In conclusion, when experimental SP1 curve and the numerical curve were compared for the same support conditions the slopes were similar.

When the capacity curves from RC walls numerical models (**Figure 10**) are analyzed, we observed a great difference in the behavior respect to the one observed in the masonry wall models. The curves of RC walls numerical models M9_C2.5_12VL (flexible base) and MBR_C2.5 (fixed base), show a wide difference in the linear slopes for as many as 15 times; we calculated 14.1 and 210 Ton/cm. Nevertheless, the rigidity values for the flexible models M10_M2.5_12VL (masonry) and M9_C2.5_12VL (RC) are close: 14.1 vs. 11.3 Ton/cm [2, 13]. The high flexibility of the slab does not allow the RC wall to develop its full strength and rigidity. This is an outstanding result that we would like to underline.

5.3 Slab-wall stiffness of specimen SP2

Figure 11a shows peak-to-peak stiffness, which is the slope of the average lateral force vs. total displacement diagram [15]. K stiffness is achieved by joining the maximum displacement points in a cycle along a straight line; the slope of the line is the cycle stiffness, and, is calculated as the difference of the shear forces, divided by the difference of displacements. **Figure 11b** shows the normalized stiffness, calculated as the peak-to-peak stiffness between the first cycle stiffness for each data series, that is, the data series stiffness for the first cycle and for the repetition cycle.

In **Figure 11b** is included the drift story limit, $\gamma = 0.006$, (indicating that nonstructural elements can be damaged). For this distortion limit value, the normalized average stiffness is approximately 35% of the initial moment of inertia, this loss of stiffness is only due to the transfer slab, because the reinforced concrete wall showed no damage. This important result should be considered in the modeling of buildings with transfer slab, so that lateral displacements can be properly calculated.

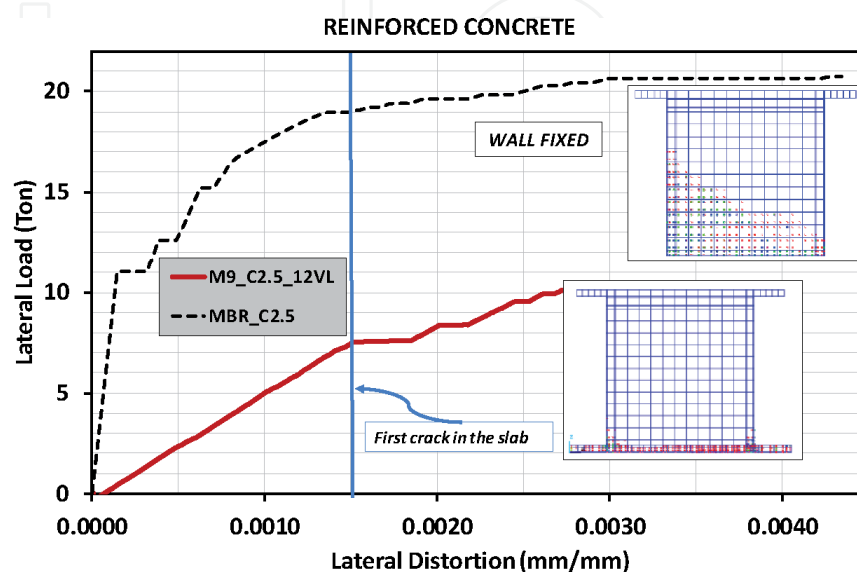


Figure 10. Load-distortion curves for M9_C2.5_12VL and MBR_C2.5 (fixed) models of RC wall, including crack patterns.

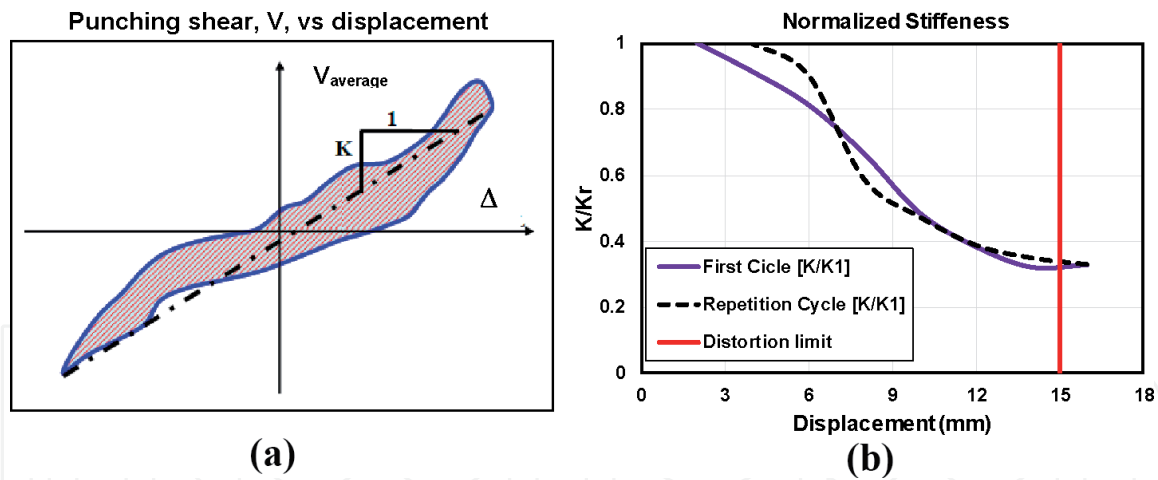


Figure 11. (a) Peak-to-peak stiffness according to Chopra [15]. (b) Normalized stiffness load-distortion curves for M9_C2.5_12VL and MBR_C2.5 (fixed) models of the concrete wall, including crack patterns.

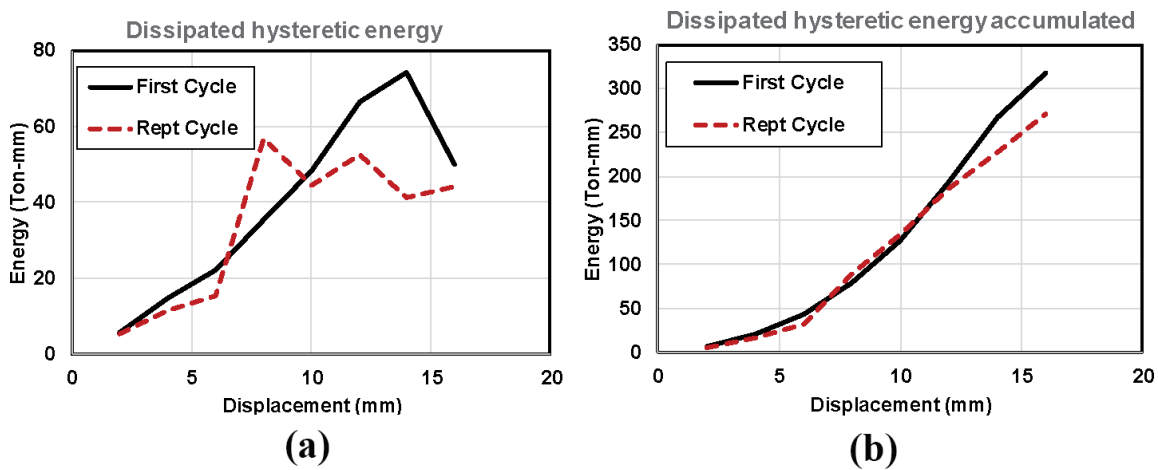


Figure 12. (a) Hysteretic energy dissipated by cycle and (b) accumulated dissipated hysteretic energy.

5.3.1 Hysteretic energy dissipated in specimen SP2

Figure 12a shows the hysteretic energy dissipated by cycle, for each data series (first cycle and repetition cycle). This energy was calculated for each cycle as the curve enclosed area "Average shear force" vs. "Total displacement" (shaded area in **Figure 11a**). It can be observed that the energy is increased with the lateral displacement. There is a change in the energy slope when the displacement is 14 mm, the energy decreases, probably due to the accumulated damage in the transfer slab. **Figure 12b** shows the accumulated dissipated hysteretic energy for each data series (first cycle and repetition cycle). It can be observed that the curve slope of the first cycle decreases, for the reasons mentioned above.

5.3.2 Equivalent viscous damping

The amount of equivalent viscous damping [15] corresponding to the energy dissipated by the structure through its nonlinear response at every cycle can be determined using the response of Specimen SP2. The equivalent viscous damping can be calculated in experimental curves, with Eq. (5). This parameter represents the internal frictions in the material [15] that, in the case of the studied specimen

SP2, the cracks are concentrated in the transfer slab. Equivalent viscous damping is estimated as:

$$\zeta_{eq} = \frac{1}{4\pi} \frac{E_D}{E_{S_0}} = \frac{1}{4\pi} \frac{\text{Energy dissipated}}{\text{Strain energy}} \quad (5)$$

Where, E_D is the energy dissipated and is calculated by the area enclosed by the hysteresis loop, and E_{S_0} is the dissipated strain energy.

Equivalent viscous damping is also used as an index that measures the damage accumulated in the member; as the crack increases, so does the damping. Mexican Building Code assumes an equivalent viscous damping equal of 5 percent of the critical, to use in seismic design. **Figure 13** shows that the average damping in the connection is about 6%, which is a value similar that assumed in traditional design.

It is also possible to estimate the ductility, which is determined from the enveloping graph of the hysteresis cycles, i.e. the curve “Lateral force” vs. “Relative displacement”. The graph is idealized as an elastoplastic curve, the elastic part is defined as the line joining the origin point of the curve with the lateral load point corresponding to two thirds of the maximum shear recorded in the test (V_{test}); the idealized plastic portion of the curve, envelope the maximum load and ends up to the ultimate displacement, which is defined as the value corresponding to 80% of the maximum resistance recorded curve. Connection ductility (μ) can be determined as the ultimate displacement (Δ_u) divided by the yielding displacement (Δ_y).

The minimum value of ductility in specimen SP2 was calculated equal to 2.19. This result illustrate that high values of ductility reduction factors cannot be adopted in the design of buildings with transfer slabs.

5.4 Analysis of crack patterns

5.4.1 Cracking in the walls

The crack pattern of masonry wall of SP1 is show in **Figure 14**, the cracks had an orientation similar with typical patterns of masonry walls subject to shear loads. This distribution of cracks is typical in confined masonry walls where the cracks are in wall diagonals, and regardless of how the wall is supported, flexible or fixed. Whereas, the crack pattern on the RC wall of specimen SP2 is illustrated in **Figure 14**, it can be observed only a few minor cracks located in the top of the wall, practically without cracks (**Figure 14**), this because the horizontal force is transmitted as a shear

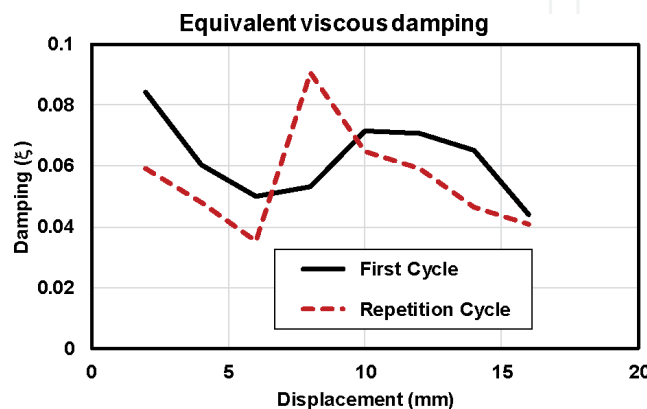


Figure 13.
 Equivalent viscous damping in specimen SP2.

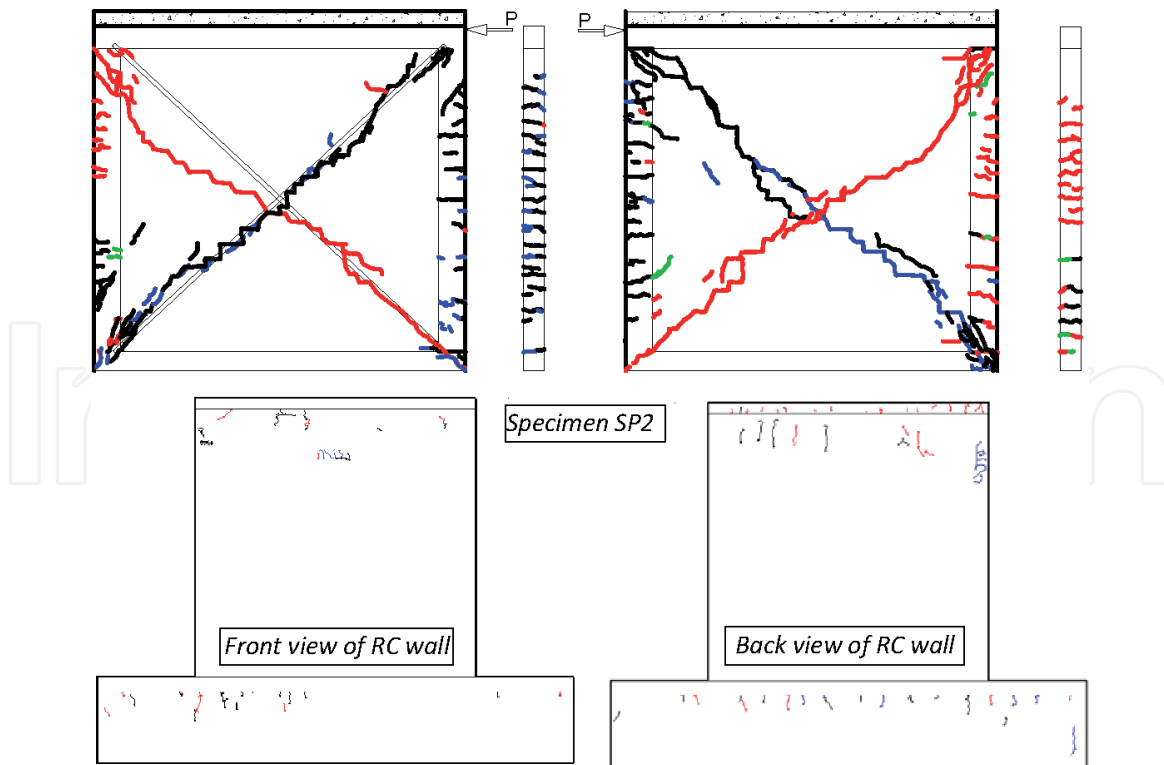


Figure 14. Cracking on the masonry wall (top) and on RC wall (bottom), after applying the complete load cycles. Cracking on the front side and back side of the wall is illustrated.

in the most resistant direction of the wall and in the slab is passed as a bending with respect to the minor inertia axis.

We also studied the pattern and distribution of cracking in the numerical models. Cracks in the masonry wall of experimental prototype SP1 are similar as the ones observed in the slab-wall numerical models. In the other hand, the behavior of the RC wall of specimen SP2 was according with the expected, it is to say, only minor cracks, the pattern is very similar with the numerical model of **Figure 10**; In the case of RC walls, the crack pattern was quite different when the base condition is analyzed; the wall on a flexible base (transfer slab) only showed a few cracks, while a wall resting on a fixed base, the crack pattern is concentrated in the tension zone of the wall (lower left corner). RC wall on a fixed support demanded its full shear capacity, while the wall on a transfer slab developed only some shear strains. This situation can be attached to the rotations of the slab, which caused a great decrease in the rigidity capacity of the entire system, **Figure 15**; a situation very delicate for the slab, particularly in the zones at the ends of the wall. The slab presented in this zone large cracks on its lower side and crushing of concrete on the upper side. This condition diminishes the slab capacity significantly (**Figure 15b**).

5.4.2 Cracking in the slabs

During the combined loading stage in prototype SP1, first cracks were detected at slab edges, close to the contiguous girders, and perpendicular to the wall. But, when the load was increased, cracks trajectories at both faces of the slab were detected (top of **Figure 15**). Cracks in the perimeter edges of upside slab were delineated, and other cracks were detected at the edges of masonry wall (**Figure 15**, top-left and bottom-left). Nevertheless, in the downside of slab, the cracks were defined as parallel lines to the walls and other lines with radial trajectories, most of these last cracks had a common origin located in the connections

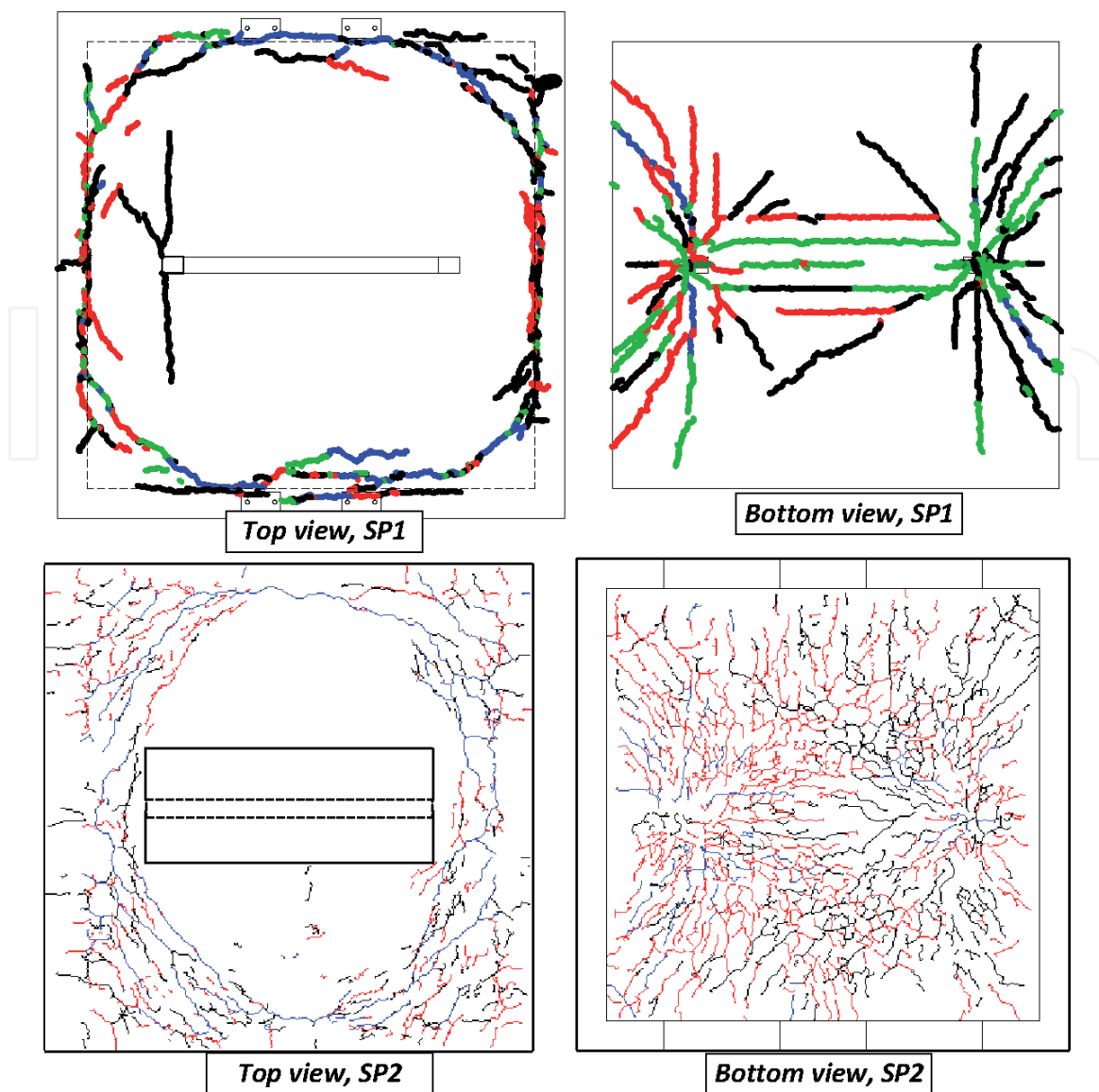


Figure 15. Cracking in the masonry wall-slab prototype SP1 (top) and cracking in the RC slab after applying the complete load cycles in the RC wall-slab prototype SP2 (bottom).

between tie-columns and slab. In the specimen SP2 (bottom of **Figure 15**) was observed a significant damage, in both sides the path of cracking was similar of SP1, however the damaged was more extensive.

5.5 Repaired specimen SP2

Due to the reinforced concrete wall was not damaged, the decision was made to repair the tested Specimen SP2. The repair consisted in the incorporation of two C shaped steel channel (**Figure 16**). The reinforcement system was designed neglecting the load capacity of the slab. Considering a vertical load of 8 Tons applied to the wall and a lateral load applied to the upper end of the wall of 6.5 Tons. The beams were considered fixed at their ends.

In the bending design of steel beams, we assumed a member with a simple section. Stud shear connectors were placed in the steel profiles to achieve a composite section (**Figure 17**). The steel profiles were fixed to the perimeter beams by steel plates that were fixed by fasteners. A space of 1 cm was left between the concrete slab and the steel profile to fill it with grout, thereby ensuring that the concrete slab is in contact with the profile along its entire length. The concrete

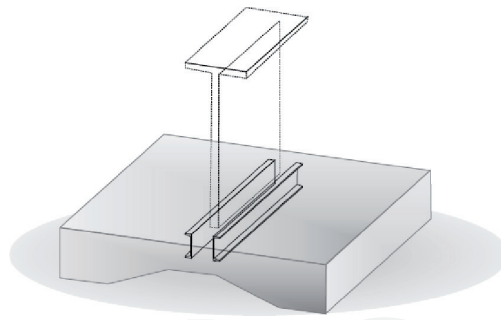


Figure 16.
Reinforcement system with two C-shaped steel channel.



Figure 17.
C-shaped steel channel with stud shear connectors (left), drills in the concrete slab.

slab was drilled so that the stud shear connectors could be placed (**Figure 16**), finally the grout was placed.

When the second specimen, SP2, is repaired, it is possible to increase some of the most important mechanical properties, such as strength, rigidity, and deformability (**Figure 18**). The resistance of the original specimen is 6.59 Tons while the resistance of the repaired specimen is 15.4 Tons, that is, it increased 2.34 times. The initial rigidity of the original specimen is 2.64 Ton/m, while the rigidity of the repaired specimen is 4.32 Ton/m, that is, an increase of 64% was achieved. The maximum displacement in the first specimen was 16.1 mm, which corresponds to a 0.6% drift ratio, the maximum drift ratio in the repaired specimen was 45.15 mm, which corresponds to a drift of 1.8%, that is, the capacity of displacement was tripled.

By neglecting the contribution of the concrete slab, a safety factor is achieved in the specimen that improves the mechanical properties.

It is concluded that the repair with steel profiles placed under the slab, is effective in improving the mechanical characteristics of rigidity, strength, and displacement capacity. This type of reinforcement can be used on transfer slabs that do not have sufficient capacity for the demands to which they can submit and prevent the damage.

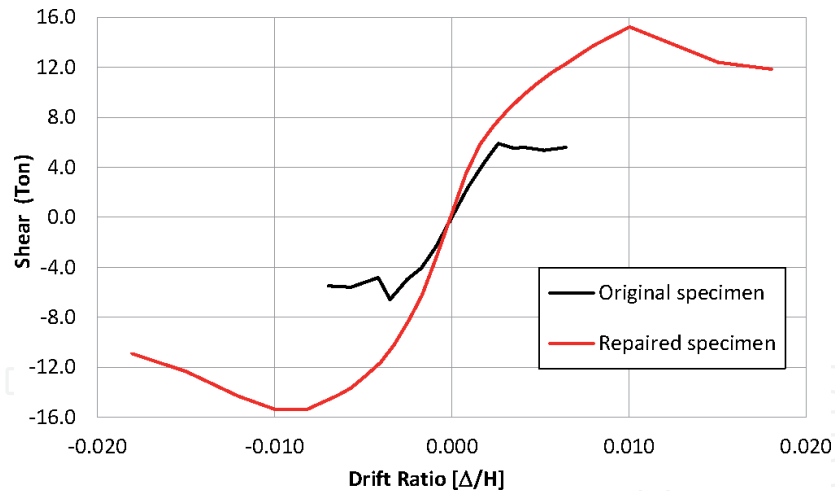


Figure 18.
 Comparison of hysteresis envelopes of the original and repaired specimen SP2.

6. Bending analysis

6.1 Measured strains and calculated bending moments

Bending moments in the two-way slab of specimen SP1 subject to the load wall can be found using the nominal moment capacity of a singly reinforced rectangular strip, with a width defined according to NTC [12], and according with the slab reinforcement of SP1 (Figure 3).

In Figure 19 are illustrated the strain variations measured from vertical load stage along the two principal central strips of SP1 slab model (longitudinal and normal wall directions). These strains were measured with the strain gages set installed in the slab (Figure 3). The first cracks in the slab (Figure 9) appeared when the vertical load reached a value of 4.8 Ton. Figure 19b also show the bending moment diagrams associated to the strains along central strips; additionally, the moment diagrams were compared with those computed using Finite Element Analysis. Maximum bending moments are in the joint of slab with tie column zone. In a lateral strip located at 75 cm from the centerline, the measured strains were approximately 60% of those of the central strip, consequently maximum negative moment also had this reduction.

In the horizontal load case, strain variations and bending moment diagrams along the center strips of two directions of the slab are shown in Figure 20; these

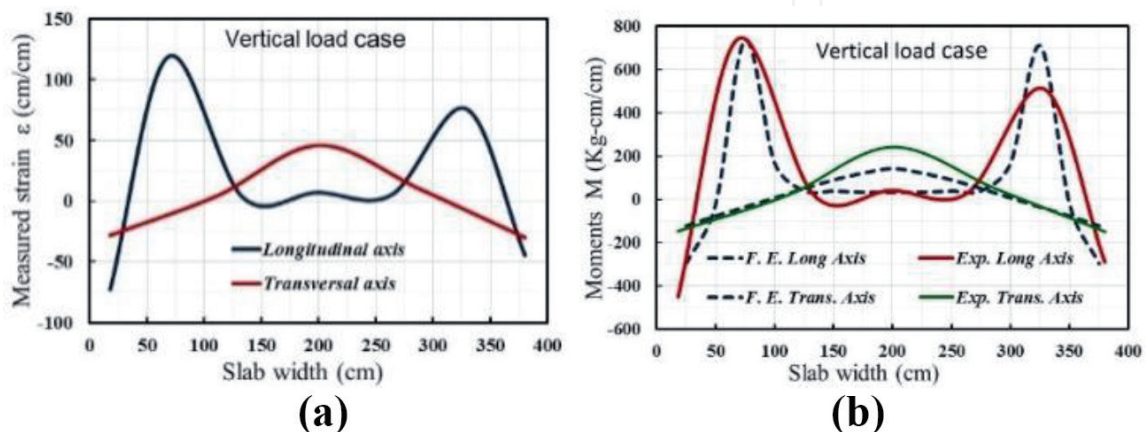


Figure 19.
 (a) Strain variations in central strip in longitudinal direction, vertical load case; (b) bending moment in central strip.

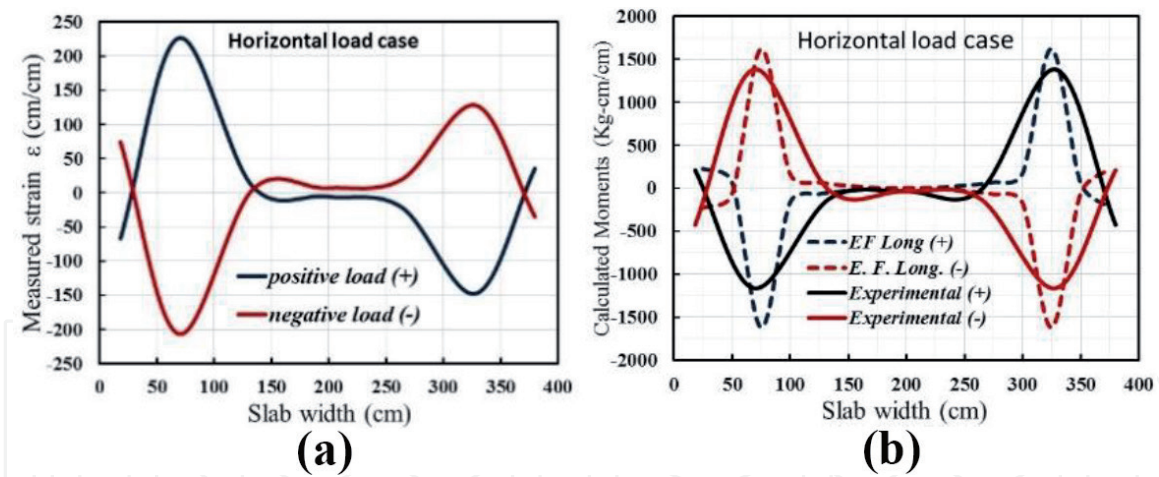


Figure 20.

(a) Strain variations in central strip from horizontal load case; (b) bending moments in central strip.

strains were obtained from the strain gages set, when the horizontal load reached 2.8 Ton. In **Figure 4b**, bending moment diagrams are compared with those computed with a finite element result. It is worth noting that, for this load level, RC slab of SP1 reached the nominal moment strength in central strip. Since maximum positive and negative bending moments are located always in the tie column zone, special design is essential in this zone when transfer slabs are used in structures.

7. Case study: a building constructed with a transfer floor system

Construction of buildings structured with transfer floor systems has become a common practice in many cities in Mexico [16] and other countries [17], some of which have a high seismic risk. To study the discontinuity effect in walls due to transfer slabs in buildings, this section presents some results from structural analysis of one real building constructed in Mexico City for residential use.

Building A has six stories on the ground level and a basement walls as part of mat Foundation. The ground story (top of **Figure 21**) is intended for parking, and their structure is based on RC frames; the five remaining stories are structured with load-bearing walls some of red brick masonry and others of reinforced concrete. Floor slabs are of various types, so the Mat foundation plate is reinforced concrete with concrete walls, the first floor (transfer slab) also is reinforced concrete cast on site, but the remaining upper levels were constructed with prefabricated beam and block, lightened with polystyrene. The plan is shown in **Figure 21**, the area enclosed by the axes A–K and 8–12, is the part of the building which rests on the transfer floor system, which is formed by beams and a solid slab of 12 cm. Most of the interior walls are interrupted at that level and do not rest on any beam (*black line* in figure).

In basis on structural analysis from the real building, shear force ratios in the masonry walls (ratio between ultimate shear and strength shear, V_u/V_D) is presented in **Figure 21**. Graphs in both directions of the building show that resistance is exceeded on a lot of discontinuous walls, and in many walls, shear force ratios are greater than 2.

8. Discussion

The main goal of the experimental program executed was to specify the behavior of wall-slab models for cyclic vertical and lateral load especially it was

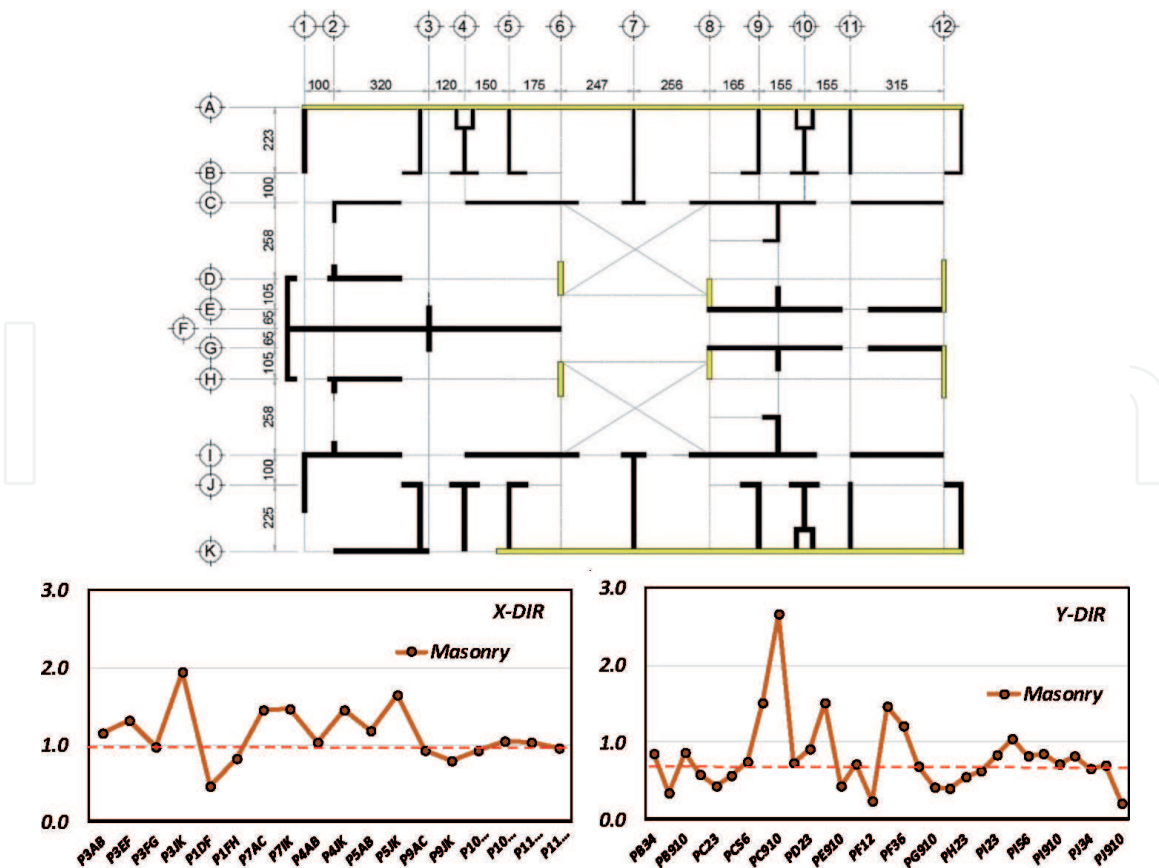


Figure 21. Transfer floor plan in building A, and shear ratio (V_u/V_D) in walls located on the transfer floor. In black line are indicated the interrupted walls in transfer slab.

demonstrated that using discontinuous walls significantly reduces the strength and rigidity of walls supported by transfer floor, which could be a design limit in practical earthquake engineering.

We propose that transfer slabs can generate the horizontal irregularity out of plane offset that can increase in a significant way the building vulnerability, this condition is different of other structural irregularities as soft story and weak story.

The most relevant finding from real buildings analysis, is that when wall discontinuity is increased, i.e., as there are more walls that are interrupted and supported on the transfer floor system, the shear and axial forces in load-bearing walls are increased too, reaching values that exceed the nominal resistance and design up to more than 3 times. Then it is recommended in the conceptual design of buildings, that the total area of discontinuous walls never can exceed 40% in a main direction; neither more than 30% in the two directions simultaneously.

Further experimental studies are needed that include other types of floor systems used in buildings such as the waffle slabs.

9. Conclusions

The findings of the experimental-analytical research program resulted in the following conclusions:

1. In the first stage, we observed the first cracking in the slab of SP1 when the vertical load reached 5.8 Tons, with a recorded deflection of 0.5 mm at the slab centerline; this load was very close to the design load from the Mexican Building Code. After the first stage, the SP1 regained its elastic behavior.

The numerical model of ANSYS also predicted the onset of cracking at the same load value.

2. Lateral stiffness of SP1 was a third part (33%) of the one observed for a wall on a fixed base. The model had horizontal displacement mainly due to slab bending (66%) and wall bending (33%). In the numerical model, the RC wall stiffness supported on a slab decreases by about 15 times due to the slab flexibility.
3. In the case of SP2, a similar loss of stiffness is observed; when the distortion limit is reached, the normalized average stiffness is approximately 35% of the initial moment of inertia.
4. We noted that the RC wall of SP2 did not show visible damage, unlike masonry wall of SP1, but in both cases, the damage to the slabs was such that these members reached a cracking condition on both slab faces. In SP1, the slab suffered a residual deformation in their center line and developed a membrane action.
5. When we analyze the results of both experimental tests, we concluded that solid slabs with small depths should not be used to transfer shear wall loads, whether masonry or CR, to nearby beams or to columns.
6. The amount of energy dissipated by the specimens was determined with the equivalent viscous damping. In SP2, the cracks were concentrated in the transfer slab. The average damping in the connection was a little more than 5% indicating that these systems dissipate a great amount of energy.
7. When are compared the curves from the experimental and numerical models, we observed an excellent correlation between these two curves.

IntechOpen

Author details

Alonso Gómez-Bernal*, Eduardo Arellano Méndez, Luis Ángel Quiroz-Guzmán, Hugón Juárez-García and Oscar González Cuevas
Universidad Autónoma Metropolitana, Azcapotzalco, México City, Mexico

*Address all correspondence to: agb@azc.uam.mx

IntechOpen

© 2020 The Author(s). Licensee IntechOpen. Distributed under the terms of the Creative Commons Attribution - NonCommercial 4.0 License (<https://creativecommons.org/licenses/by-nc/4.0/>), which permits use, distribution and reproduction for non-commercial purposes, provided the original is properly cited. 

References

- [1] Gómez Bernal A, Juárez García H, Roldán Islas J. Earthquake damage due to soft soil conditions and structural features of the building infrastructure in La Colonia Roma, Mexico City. In: 6th Structural Engineers World Congress 6SEWC. Cancún, QR, México: Structural Engineering Worldwide; 2017
- [2] Gomez-Bernal A, Manzanaras DA, Juarez-Garcia H. Interaction between shear walls and transfer-slabs, subjected to lateral and vertical loading. In: Proc. Vienna Congress on Recent Advances in Earthquake Engineering and Struc. Dynamics Pap 447, Vienna, Aut. 2013. pp. 28-30
- [3] Roeslin S, Elwood KJ, Juarez-Garcia H, Gomez-Bernal A, Dhakal RP. The September 19th, 2017 Puebla, Mexico earthquake. In: Proceedings of the New Zealand Society for Earthquake Engineering Annual Technical Conference. Auckland, New Zealand. 2018. Available from: <https://researchspace.auckland.ac.nz/handle/2292/44962>
- [4] Carrillo J, Alcocer S, González G. Deformation analysis of concrete walls under shaking table excitations. *J. DYNA*. 2012;**79**(174):145-155. ISSN: 0012-7353
- [5] Gouveia JP, Lourenço PB. Masonry shear walls subjected to cyclic loading: Influence of confinement and horizontal reinforcement. In: Proc. Tenth North American Masonry Conference, St. Louis, USA. 2007
- [6] Preti M, Migliorati L, Giuriani E. Experimental testing of engineered masonry infill walls for post-earthquake structural damage control. *Bulletin of Earthquake Engineering*. 2015;**13**(7):2029-2049. DOI: 10.1007/s10518-014-9701-2
- [7] Haris I, Farkas G. Experimental results on masonry infilled RC frames for monotonic increasing and cyclic lateral load. *Periodica Polytechnica Civil Engineering*. 2018;**62**(3):1-11. DOI: 10.3311/PPci.10715
- [8] Meli R. Mampostería estructural, la práctica, la investigación y el comportamiento sísmico observado en México. CENAPRED reporte Seguridad sísmica de la vivienda económica, n.17 julio. México; 1994
- [9] Park R, Gamble WL. *Concrete Slabs*. 2nd ed. New York, USA: Wiley & Sons Inc; 2000
- [10] Vecchio F, Tang K. Membrane action in reinforced concrete slab. *Canadian Journal of Civil Engineering*. 1990;**17**:686-697
- [11] Xiao Y, Li B, Fujikake K. Experimental study of reinforced concrete slabs under different loading rates. *Structural Journal*. 2016;**113**(1):157-168. DOI: 10.14359/51688067
- [12] Reglamento de Construcciones del Distrito Federal. NTC de Mampostería. Gaceta Oficial del Gobierno CDMX, México; 2017
- [13] Gómez-Bernal A, Manzanaras D, Vargas O, Arellano-Méndez E, Juárez-García H, González-Cuevas O. Experimental behavior of a masonry wall supported on a RC two-way slab. *J. DYNA*. 2015;**82**(194):96-103. DOI: 10.15446/dyna.v82n194.46333
- [14] Tickoo S, Singh V. ANSYS 11.0 for Designers, CAD/CIM Technologies, 2009
- [15] Chopra AK. *Dynamics of Structures*. 4th ed. Pearson; 2012
- [16] Gómez Bernal A, Juárez García H, Alcántara P, Roldán Islas J. Vulnerability

of buildings with out of plane offsets
irregularity constructed in México. In:
Proc. XVI World Conf. on Earthquake
Engineering, WCEE, Santiago Chile.
2017

[17] Lande PS, Takale P. Analysis
of high-rise building with transfer
floor. International Research Journal
of Engineering and Technology.
2018;05(5):2483-2488. e-ISSN:
2395-0056

IntechOpen